

Planar lattice model with gas, liquid, and solid phases

Douglas Poland

Department of Chemistry, The Johns Hopkins University, Baltimore, Maryland 21218

(Received 15 June 1998)

We treat a lattice gas model on the planar-honeycomb lattice with nearest-neighbor exclusion and two types of next-nearest-neighbor attraction. In the generalized Bethe approximation described in the previous paper, the model exhibits both a gas-liquid, Ising-like, phase transition (with a critical point) and a gas-solid phase transition. We show that the qualitative features of the activity-temperature gas/liquid/solid phase diagram found in the Bethe approximation are present in a more rigorous treatment of the model using exact series expansions. [S1063-651X(99)09102-3]

PACS number(s): 05.20.-y, 05.50.+q, 05.70.Fh, 05.70.Jk

I. INTRODUCTION

In the present paper we treat a lattice gas model on the planar honeycomb lattice that in the generalized Bethe approximation developed in the previous paper [1] clearly displays gas, liquid, and solid phases with a gas-liquid critical point. We also use exact series expansions to corroborate the existence of canonical three-phase behavior in this model.

To understand the motivation for choosing a particular lattice gas model that is likely to exhibit gas, liquid, and solid phases we need to review some of the basic facts about lattice gases in general. We take the view that the lattice is a device that allows us to construct a discrete approximation to the configuration integral in continuous space and that the main ingredient in the cooperative behavior between molecules is, as one moves out from the center of a reference molecule, a range of infinitely repulsive interactions (excluded volume effect) followed by a range of attractive interactions the strength of which rapidly go to zero far from the center of the reference molecule. Figure 1 illustrates how repulsion and attraction are incorporated into simple lattice models. Figure 1(a) illustrates the simplest lattice-gas model, the Ising model on the planar-square lattice, where the range of exclusion is shown by the inner circle and encompasses just a single site while the range of attraction is the four nearest-neighbor sites shown in the outer circle. If one keeps the size of the regions in the concentric circles in Fig. 1(a) fixed and decreases the lattice spacing by a factor of two one gets the lattice gas shown in Fig. 1(b). If one kept decreasing the lattice spacing then the properties of the lattice gas would (slowly) approach the behavior of system in continuous space. Of course the reason for using the lattice-gas system is that it is much simpler to treat than the system in continuous space. And renormalization-group theory tells us that the essential features of a system (particularly the nature of the critical point) are insensitive to the scale of the system. The hope is that the lattice gas will exhibit behavior that is qualitatively similar to that of the continuous system. From the work of Onsager [2] we know that the model shown in Fig. 1(a) exhibits a gas-liquid phase diagram with a critical point. There is evidence in the literature [3], based on studies of finite chunks of lattice, that a model like that shown in Fig. 1(b) will show three-phase behavior. We are seeking a model that is complicated enough to show canonical three-phase

behavior but simple enough to be amenable to study using exact series.

A central problem with lattice gases is that the lattice seems to introduce an artificial order in that at high density all lattice gases look like a regular solid. But in fact the most famous lattice gas, the Ising model illustrated in Fig. 1(a), is not a gas-solid model, but a gas-liquid model and the high-density phase in the Ising model is a model of a liquid, not a solid. To understand why this is so one must focus on the central feature of all Ising models and that is that the range of excluded volume extends only to a single lattice site. Lee and Yang [4] generalized the notion of an Ising model by allowing any number of attractive interactions, as illustrated in

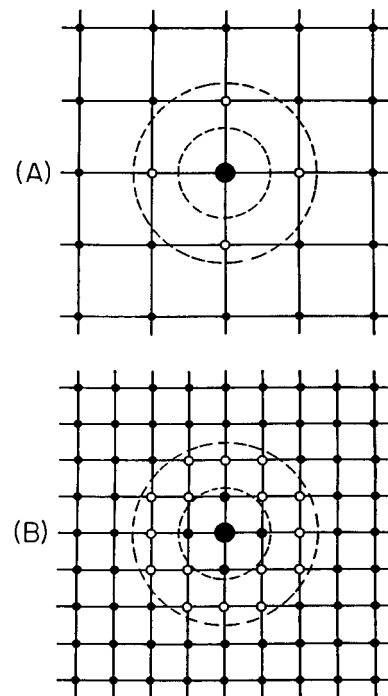


FIG. 1. Illustration of regions of repulsion and attraction around a particle in lattice gases. (a) The standard nearest-neighbor Ising model where only the central site is excluded and attraction is felt on nearest-neighbor sites (open circles). (b) The same model as in (a) except that the lattice grid has been made twice as fine. Now there are five excluded sites (solid circles) and nine sites for attraction (open circles).

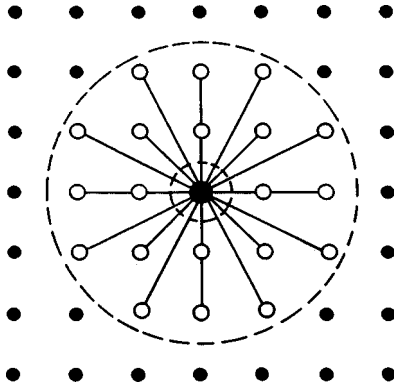


FIG. 2. Schematic illustration of the generalized Lee-Yang Ising model having extensive sites for attractive interactions (open circles) which are not necessarily of the same intensity, but where only the central site is excluded. This kind of model at most exhibits two phases with an Ising-like, gas-liquid phase diagram.

Fig. 2, but kept the feature of single site exclusion. With a properly defined fugacity (scaled activity), the roots of the grand partition function for the generalized Ising model all are on the unit circle and, as the temperature is decreased, come from the negative real-fugacity axis around the unit circle, and at the critical point, touch the positive real-fugacity axis. The unit circle cuts the positive fugacity axis only once and thus there is one and only one singularity (phase transition) in generalized Ising models and it mimics the gas-liquid system with a first-order phase transition ending at a critical point. The high-density phase is not a solid since there is no interaction forcing the particles to take up positions on a particular sublattice of sites. Thus no matter how many attractive interactions one introduces, as in Fig. 2, as long as there is only a single, central excluded site the model display gas-liquid behavior.

As soon as the range of exclusion goes beyond the central site, as in the model shown in Fig. 1(b), then one has a gas-solid model. The reason for this is that when one has nearest-neighbor exclusion the particles are forced to occupy every other site at very high density and there are two ways of doing this, either on sublattice (a) or (b), as discussed in the previous paper. The onset of sublattice order is then the determining feature of a solid phase in a lattice gas.

To be more explicit in describing the phase-diagrams involved in various lattice models we need to define a few variables. The first of the basic thermodynamic quantities we need is the activity

$$z = \exp[\beta\mu - \beta\mu_0], \quad (1.1)$$

where $\beta = 1/kT$ (where kT has the usual meaning) and μ is the chemical potential (with μ_0 the standard chemical potential). With the definition of Eq. (1.1) one has

$$z \sim \rho \quad \text{as } \rho \rightarrow 0, \quad (1.2)$$

where ρ is the number density of particles on the lattice. The second quantity we need is the Boltzmann factor for attractive interactions,

$$x = \exp[-\beta\varepsilon], \quad (1.3)$$

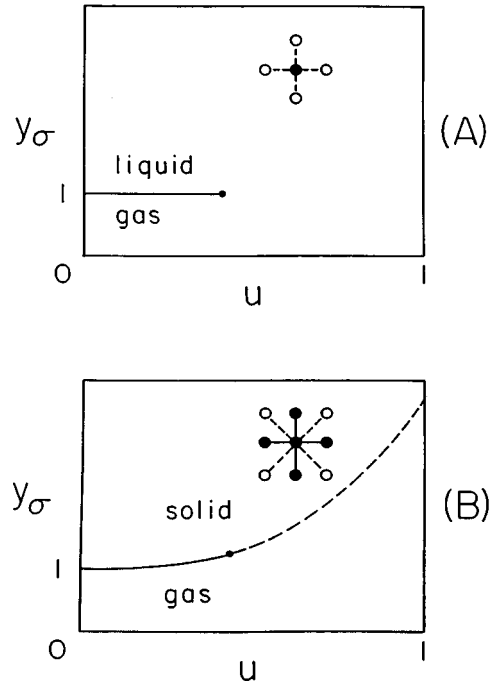


FIG. 3. Schematic illustration of $y_\sigma(u)$, the locus where y exhibits a phase-transition singularity as a function of u . (a) The nearest-neighbor Ising model illustrating a gas-liquid phase diagram. (b) The model of nearest-neighbor exclusion and next-nearest-neighbor attraction (discussed in Ref. [1]) illustrating a gas-solid phase diagram. In the schematic insets the solid circles represent excluded sites and the open circles represent sites for attractive interactions.

where ε is the negative (for attractions) interaction energy. It is also useful to define the inverse of x ,

$$u = 1/x, \quad (1.4)$$

which is a low-temperature parameter since $u \rightarrow 0$ as $T \rightarrow 0$; $u = x = 1$ when $T \rightarrow \infty$.

A variable that is central to our discussion is the scaled activity or fugacity, which involves both z and x . For the planar-square lattice illustrated in Fig. 1(a) this quantity is

$$y = zx^2. \quad (1.5)$$

The motivation for this definition of y is that in the close-packed limit the grand partition function for the system, using the example just mentioned, is

$$\Xi_{\text{close packed}} = y^M \quad (1.6)$$

for a lattice of M sites. Note that the definition of y in Eq. (1.5) uses x^2 and not x^4 since each of the four bonds per particle is shared by two particles. Since for the empty lattice

$$\Xi_{\text{vacant}} = 1, \quad (1.7)$$

one anticipates that when $y = 1$ interesting things will happen (since this is the balance point between the empty and full lattice) and indeed this was proved for all Ising models by Lee and Yang [4]. The exact definition of y , as given in Eq. (1.5), will depend on the model.

In Fig. 3(a) we illustrate the locus of the phase transition

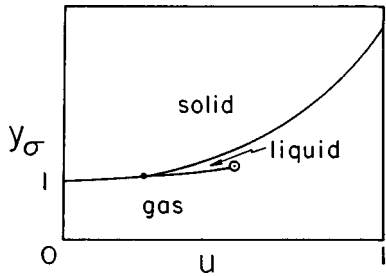


FIG. 4. Schematic illustration of the $y_\sigma(u)$ phase diagram for a substance exhibiting the gas, liquid, and solid phases. The three phases coexist at the triple point (solid circle). The critical point is indicated with an open circle. (a), (b), and (c) indicate parts of the y_σ loci that can be located using different series techniques.

singularities in the fugacity y_σ for the Ising model (single-site exclusion, nearest-neighbor attraction). The locus is $y_\sigma = 1$ from absolute zero ($u=0$) up to the critical point where the y_σ locus separates the gas and liquid phases. In Fig. 3(b) we illustrate y_σ for the lattice gas with nearest-neighbor exclusion and next-nearest-neighbor attraction. In this case the locus extends from absolute zero up to infinite temperature ($u=1$). The dashed portion of the curve indicates the line of second-order transitions, the transition being first order below the tricritical point. In the latter model the attractive interactions enforce the sublattice ordering and hence there are only the gas and solid phases in this model, with no liquid phase.

Clearly the idea is to combine the behaviors shown in Figs. 3(a) and 3(b) together so that one has gas, liquid, and solid behavior in one model. Figure 4 schematically shows the y_σ locus we would like to find. As long as one has nearest-neighbor exclusion one will have solidlike sublattice order at high densities and so the gas-solid part is easy. The problem is to reintroduce Ising-like gas-liquid behavior with an ordinary critical point. The straightforward way to do this seems to be to introduce a variety of attractive interactions, not all of which reinforce the sublattice structure. The model we have chosen is shown in Fig. 5. It is a lattice gas on the planar hexagonal lattice with nearest-neighbor exclusion (the

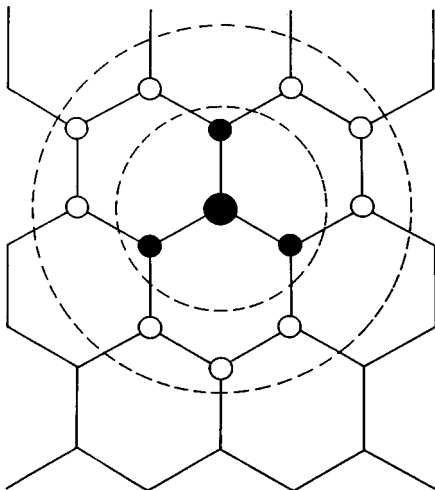


FIG. 5. The honeycomb lattice model. The solid circles represent excluded sites while the open circles represent sites for attractive interactions.

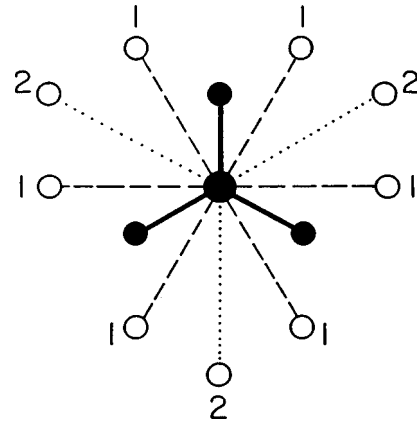


FIG. 6. A reproduction of Fig. 5 with the two types of site for attractive interactions labeled as 1 and 2.

inner circle of dark circles) and next-nearest-neighbor interactions (the outer circle of open circles) of two types. The types of interaction are illustrated in Fig. 6 with the excluded sites indicated by dark circles and the attractive sites by open circles, with the two types labeled by 1 and 2. We will define the Boltzmann factors for the two types of attractive interactions as

$$x = \exp[-\varepsilon_1/kT] \quad \text{and} \quad v = \exp[-\varepsilon_2/kT]. \quad (1.8)$$

At high density the particles take up a sublattice order, illustrated in Fig. 7; the sublattice order is reinforced by the shorter attractive interactions (the x factors) and a few are illustrated by dashed lines in Fig. 7. The fact that there are two types of attractive interactions leads to clusters having very different geometries. If one uses all x -type interactions then one gets clusters of the form shown in Fig. 8(a) (with a triangular geometry) while if one uses all v -type interactions one gets clusters of the form shown in Fig. 8(c) (with a hexagonal geometry). If one uses both types of interaction then one gets the irregular networks shown in Fig. 8(b) and the hope is that the entropy associated with the irregular networks will give the model gas-liquid behavior at intermediate densities.

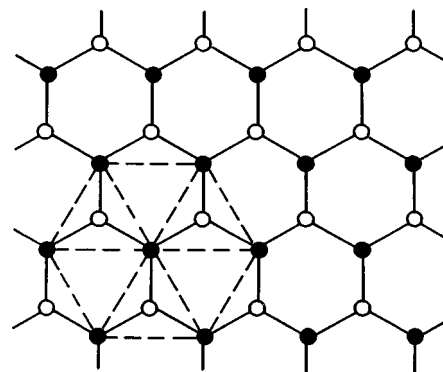


FIG. 7. Illustration of the close-packed structure for the honeycomb model of Fig. 5. As a result of the nearest-neighbor exclusions, particles (shown by solid circles) must exist on a sublattice consisting of every other lattice site. The next-nearest-neighbor attractive interactions are shown by dashed lines (which show that the sublattice of the honeycomb lattice defines a triangular lattice).

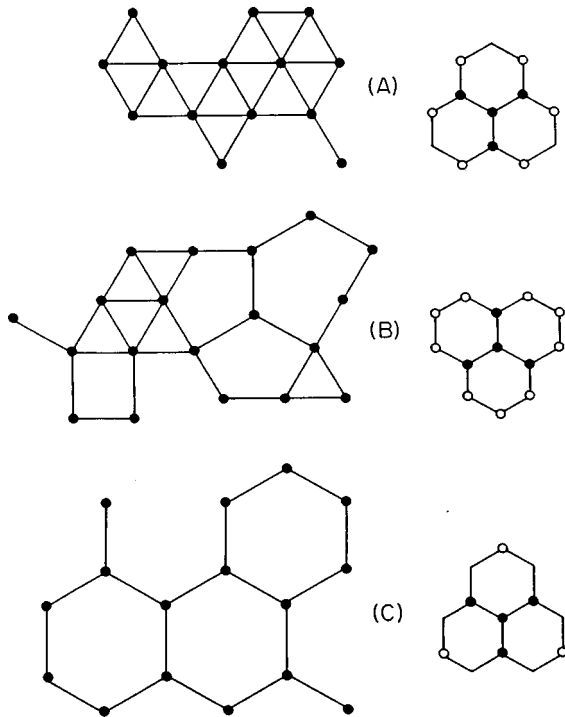


FIG. 8. Possible compact clusters in the honeycomb lattice model. (a) A cluster with triangular geometry formed using type-1 interactions only. (b) An irregular cluster formed using both type-1 and type-2 interactions. (c) A cluster with super-honeycomb geometry formed using type-2 interactions only. The insets illustrate the type of attractive interactions (open circles) used to generate the clusters; the excluded sites (solid circles) are the same in all cases.

There are two simple ordered structures possible with the two types of attractive interactions introduced. Starting with the basic honeycomb lattice illustrated in Fig. 9(a) one gets a regular but very open solid with honeycomb geometry illustrated in Fig. 9(b). The triangular-type solid, already illustrated in Fig. 7, is shown again in Fig. 9(c). The portions of dashed lattice shown in (II) and (III) indicate the geometry of the original honeycomb lattice. We want the triangular-type solid to be the most stable form as the temperature goes to absolute zero. To discuss the relative stability of the various solid phases shown in Fig. 9 it is useful to write interaction v in terms of interaction x as follows:

$$v = x^\kappa. \quad (1.9)$$

Then the grand partition functions for the regular systems of the empty lattice, honeycomb-type solid, and triangular-type solid are, respectively,

$$\Xi_0 = 1, \quad \Xi_h = (zx^{3\kappa/2})^{M/4}, \quad \Xi_t = (zx^3)^{M/2}. \quad (1.10)$$

We let M be the number of lattice sites on the original lattice; there are then $M/4$ particles on the superhoneycomb lattice [Fig. 9(b)] and $M/2$ particles on the triangular lattice [Fig. 9(c)]. We define a fugacity relative to the triangular-type solid phase (where z is the activity),

$$y = zx^3. \quad (1.11)$$

In the triangular-type solid phase of Fig. 7 there are six of the x -type interactions per particle, but each bond is shared by

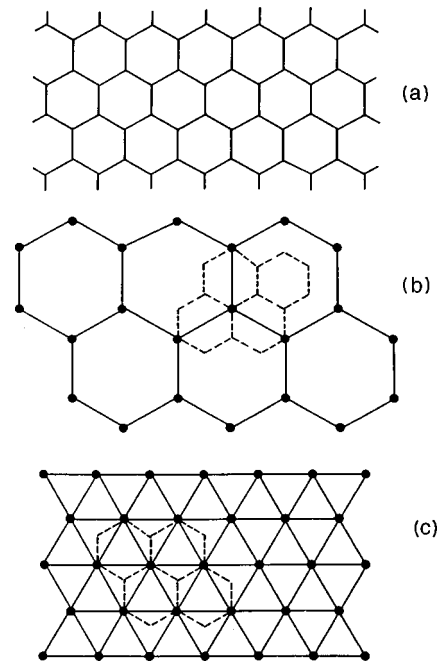


FIG. 9. Three types of regular lattice configuration for the honeycomb lattice gas model. (a) The empty lattice. (b) The superhoneycomb configuration resulting from utilizing type-2 interactions only. (c) The triangular configuration resulting from utilizing type-1 interactions only. In (b) and (c) a portion of the underlying honeycomb lattice is shown using dashed lines. When $\kappa=2$ all three configurations are equally probable at $u=0$ (absolute zero).

two particles and hence the definition of Eq. (1.11). In terms of y the grand partition functions of Eq. (1.10) become

$$\Xi_0 = 1, \quad \Xi_h = [y/x^{3/2(2-\kappa)}]^{M/4}, \quad \Xi_t = y^{M/2}. \quad (1.12)$$

In general for this class of models the phase transition locus will not be $y_\sigma = 1$, as in generalized Ising models, but, anticipating Eq. (4.19), $y_\sigma \rightarrow 1$ as $T \rightarrow 0$ ($u \rightarrow 0$). Thus for the triangular-type solid to be the most stable at absolute zero we require

$$\Xi_t > \Xi_h, \quad (1.13)$$

or from Eq. (1.12) setting $y = 1$,

$$\kappa < 2. \quad (1.14)$$

For manipulations with series it is useful to have κ a rational fraction. Explorations of the behavior of models with κ near 2 show that the following value of κ gives interesting results:

$$\kappa = 9/5, \quad (1.15)$$

or introducing a parameter w ,

$$x = w^5 \quad \text{and} \quad v = w^9 = x^{9/5}. \quad (1.16)$$

The choice of $\kappa = \frac{9}{5}$ guarantees that the triangular-type solid of Fig. 9(c) will be the stable phase at high density. Since $v > x$, the dominant dimers formed at low density will utilize the v interaction (h type) rather than the t type. At intermediate densities there will be a mixture of the two

types (we will show this quantitatively in Fig. 26). We will refer to the choice of parameters given in Eqs. (1.15) and (1.16) as the $\frac{9}{5}$ model.

We now show that in the generalized Bethe approximation this model shows gas-liquid-solid behavior. A key ingredient in the generalized Bethe approximation is the behavior at high temperature ($x=v=1$) where the model has just the hard core exclusion and we turn to that limit first.

II. HIGH-TEMPERATURE LIMIT

In the high-temperature limit when $x=v=1$ we have the model of nearest-neighbor exclusion on the honeycomb lattice. In analogy with the behavior of the similar model on the square-planar lattice [5–7], we expect a second-order phase transition at high density where sublattice order begins. The second-order transition will occur at a critical density ρ_σ and a critical value of the activity, z_σ . The simplest way to determine these parameters is by using high-density series, which are essentially perturbation series about the close-packed lattice (as illustrated in Fig. 7). High-density series are very sensitive to sublattice order and hence allow us to determine the critical parameters easily. We will defer a discussion of the calculation of the series until a later section and here simply quote the results. The high-density series for the pressure is given in inverse powers of the activity. The series through eight terms is

$$\begin{aligned} \beta p_H(z) = & \frac{1}{2} \ln(z) + \frac{1}{2} [z^{-1} + \frac{1}{2} z^{-2} + 1 \frac{1}{3} z^{-3} + 4 \frac{1}{4} z^{-4} \\ & + 16 \frac{1}{5} z^{-5} + 72 \frac{2}{3} z^{-6} + 355 \frac{1}{7} z^{-7} + 1843 \frac{1}{8} z^{-8} + \dots]. \end{aligned} \quad (2.1)$$

The density and modified compressibility are given in general by

$$\rho = \frac{\partial \beta p}{\partial \ln z} \quad \text{and} \quad \chi = \frac{\partial \rho}{\partial \ln z}. \quad (2.2)$$

The modified compressibility is related to the standard isothermal compressibility K_T by the relation $K_T = \chi / (kT\rho^2)$. It is convenient to introduce the relative density of holes,

$$\rho' = 1 - 2\rho. \quad (2.3)$$

Using the above expressions we can obtain both the activity and density series for χ_H (the compressibility obtained from the high-density series),

$$\begin{aligned} \chi_H(z^{-1}) = & z^{-1} + 2z^{-2} + 12z^{-3} + 68z^{-4} + 405z^{-5} \\ & + 2616z^{-6} + 17,402z^{-7} + 117,960z^{-8} + \dots, \end{aligned} \quad (2.4)$$

$$\begin{aligned} \chi_H(\rho') = & \rho' + (\rho')^2 + 6(\rho')^3 + 24(\rho')^4 + 96(\rho')^5 \\ & + 504(\rho')^6 + 2532(\rho')^7 + 12,296(\rho')^8 + \dots. \end{aligned} \quad (2.5)$$

Both series are very well behaved and clearly diverge at critical values of the activity and density respectively (z_σ and ρ_σ). The points of divergence are easily located using Padé

approximants to the series. First we will convert the function under consideration to the logarithmic derivative,

$$D \ln \chi(z) = \frac{\partial \ln \chi}{\partial \ln z}, \quad (2.6)$$

which converts singularities of the form $(z_\sigma - z)^{-\gamma}$ to simple poles, which are then determined by forming a Padé approximant (a ratio of finite polynomials) and locating the roots of the denominator polynomial. The off-diagonal Padé approximants to the activity and density series for $D \ln \chi_H$ give

$$\begin{aligned} z_\sigma = & 7.56, \quad 7.55, \\ \rho_\sigma = & 0.411, \quad 0.411. \end{aligned} \quad (2.7)$$

On the square-planar lattice with nearest-neighbor exclusions only we have found [7]

$$\chi_H \sim -\ln[1/z_\sigma - 1/z]. \quad (2.8)$$

Assuming this also holds on the honeycomb lattice we expect

$$\frac{\partial \chi_H}{\partial \ln z} \sim \frac{1}{1/z_\sigma - 1/z}. \quad (2.9)$$

If the above function exhibits a simple pole then the ratios of consecutive terms should be constant and equal to z_σ . The ratios are 4.00, 9.00, 7.56, 7.44, 7.75, 7.76, and 7.75; clearly the form of Eq. (2.8) is strongly supported. For numerical estimates the results of the Padé approximants of Eq. (2.7) are more reliable since these results are not influenced by nearby singularities.

Double-activity series, in which particles are labeled according to the sublattice on which they are located, are very sensitive to the breakdown of sublattice order. We define the high-density double-activity series for the pressure as follows:

$$\beta p_H(z_A, z_B) = \frac{1}{2} \left[\ln(z_A) + \sum_n b'_n(s) (1/z_A)^n \right], \quad (2.10)$$

where

$$b'_n(s) = \sum_k b_{n,k} s^k \quad (2.11a)$$

and

$$s = z_B / z_A. \quad (2.11b)$$

The $(1/z_A)$ parameter keeps track of how many particles have been removed from the A sublattice while the number of s factors tells how many particles have been moved from the A to the B sublattice. The first six b'_n are given below for the planar-honeycomb lattice with nearest-neighbor exclusion:

$$b'_1 = 1, \quad b'_2 = -\left(\frac{1}{2}\right) + s$$

$$b'_3 = \left(\frac{1}{3}\right) - 3s + 3s^2 + s^3$$

$$b'_4 = -\left(\frac{1}{4}\right) + 6s - 18\left(\frac{1}{2}\right)s^2 + 4s^3 + 9s^4 + 3s^5 + s^6, \quad (2.12)$$

$$b'_5 = \left(\frac{1}{5}\right) - 10s + 66s^2 - 79s^3 - 49s^4 + 27s^5 + 26s^6 + 22s^7 \\ + 9s^8 + 3s^9 + s^{10},$$

$$b'_6 = -\left(\frac{1}{6}\right) + 15s - 178\left(\frac{1}{2}\right)s^2 + 483\left(\frac{1}{3}\right)s^3 - 73\left(\frac{1}{2}\right)s^4 - 456s^5 \\ - 112\left(\frac{1}{2}\right)s^6 + 117s^8 + 117s^9 + 75s^{10} + 51s^{11} + 22s^{12} \\ + 9s^{13} + 3s^{14} + s^{15}.$$

In the series for b'_6 there is no s^7 term and the coefficients for the s^8 and s^9 terms are the same.

The coefficients in Eq. (2.12) show that sublattice order breaks down rapidly on the honeycomb lattice as particles are removed from the close-packed structure. For example, in b'_6 there are s^k terms through $k=15$ which means that if six particles are removed from the dominant sublattice, as many as fifteen particles can be shifted onto the other sublattice. We discuss the high-density series further in Sec. IV; there we will illustrate (in Fig. 21) the origin of the s^6 term in b'_4 , this term representing the removal of four particles from the A sublattice and the movement of six particles from the A to the B sublattice.

Using the sublattice-activity series of Eq. (2.10) we can calculate the appropriate order parameter

$$R = 2(\rho_A - \rho_B), \quad (2.13)$$

where

$$\rho_A = \frac{\partial \beta p_H}{\partial \ln z_A} \quad \text{and} \quad \rho_B = \frac{\partial \beta p_H}{\partial \ln z_B}. \quad (2.14)$$

After taking the derivatives in Eq. (2.14) we set $z_A = z_B = z$ (there is, after all, only one activity), we have the z and ρ' series for R ,

$$R(z^{-1}) = 1 - [z^{-1} + 3z^{-2} + 16z^{-3} + 93z^{-4} \\ + 567z^{-5} + 3630z^{-6} + \dots], \\ R(\rho') = 1 - [(\rho') + 2(\rho')^2 + 8(\rho')^3 + 34(\rho')^4 \\ + 146(\rho')^5 + 684(\rho')^6 + \dots]. \quad (2.15)$$

We can estimate the point at which R goes to zero (the second-order transition marking the end of sublattice order) by calculating the values of $(1/z)$ and ρ' that make successive truncations of the series become zero. The values are (for truncations at the first through the sixth power of the appropriate variable):

$$(1/z)_0 = 1, 2.30, 3.34, 4.07, 4.60, 5.01, \\ (\rho')_0 = 0, 0.250, 0.319, 0.348, 0.363, 0.372. \quad (2.16)$$

These values are seen to be extrapolating smoothly to the numbers given in Eq. (2.7) determined from χ_H .

Having located the second order transition for the high-temperature gas-solid transition we can now use a Padé ap-

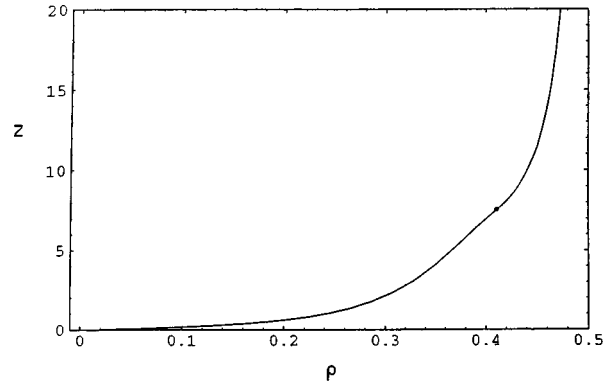


FIG. 10. The quantity p/kT as a function of density in the high-temperature limit for the honeycomb lattice with nearest-neighbor exclusion. The solid dot indicates the location of the second-order transition that accompanies the onset of sublattice order as the density is increased. The curves on either side of the transition are Padé approximants to the low- and high-density series.

proximant to the high-density activity series for the pressure of (2.1) for activities and densities on the high density side of the transition. For the low-density activity series for the pressure and the density we can use the part of the Ising-series for the honeycomb lattice appropriate to the high-temperature limit. These quantities are known through 21st term [8,9], the first few being given below:

$$\beta p_L(z) = z - 4z^2 + 19z^3 - 98z^4 \\ + 531z^5 - 2971z^6 + \dots. \quad (2.17)$$

The density as a function of the activity is given by a relation analogous to that given in Eq. (2.2). That relation can then be inverted to give the pressure and the activity as a series in the density. Since we have only eight terms in the high-density series we find that the best fit between the low- and high-density ends comes when we use an $(\frac{8}{8})$ Padé approximant for the pressure and an $(\frac{7}{7})$ approximant for the activity. The low and high density branches of these functions do not match exactly at $\rho_\sigma = 0.411$ and $z_\sigma = 7.55$ [the low density values for the pressure (βp) and the activity are 1.062 and 7.55, respectively, while the corresponding values on the high density side are 1.089 and 7.69]. To avoid an artificial jump in the curves we add in a small correction term in $(\rho')^9$ for the high-density functions. This is a minor correction that gives us a continuous curve for the pressure and the activity as a function of density over the whole range of the density. The Padé approximants to the high- and low-density functions are shown in Fig. 10 (for the activity as a function of density) and in Fig. 11 (for the pressure as a function of the density). The location of the second-order transition is indicated with a solid dot in both and is seen to be a subtle inflection in each curve. Having a workable function for the pressure and the activity as a function of density we can now use the generalized Bethe approximation to treat our honeycomb model.

III. BEHAVIOR IN THE GENERALIZED BETHE APPROXIMATION

In Fig. 12 we show the lattice block (three joined hexagons) that we will use for the Bethe approximation for the

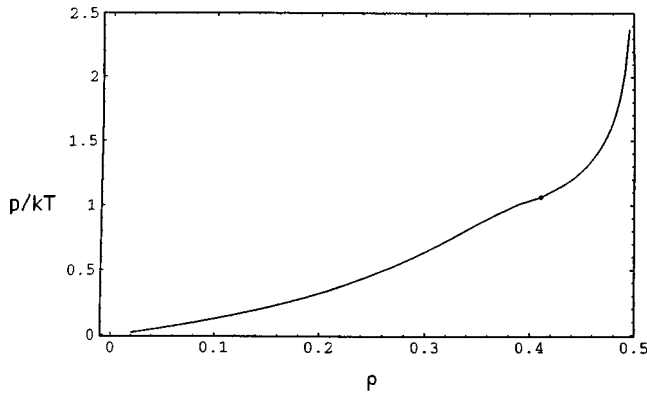


FIG. 11. The activity z as a function of density in the high-temperature limit for the honeycomb lattice with nearest-neighbor exclusion. The solid dot indicates the location of the second-order transition that accompanies the onset of sublattice order as the density is increased. The curves on either side of the transition are Padé approximants to the low- and high-density series.

honey comb model. It was chosen since it contains all of the interactions shown in Figs. 5 and 6. How the plane can be tiled with these blocks is also shown. The numbers on the single block indicate the fraction of each site that is assigned to the given block; there is one site (the central) that is entirely inside the block (1) while there are three sites that belong $\frac{2}{3}$ to the block and nine sites that belong $\frac{1}{3}$ to the block. These numbers are the α 's of the previous paper [1]. Using the $\kappa = \frac{9}{5}$ model of Eqs. (1.15) and (1.16) we then apply the procedure of the previous paper. We find that there is an Ising-like critical point in the model that occurs at $x_c = 2.64$. Figure 13 shows the density as a function of y [defined in Eq. (1.5)] for $x < x_c$ ($x = 2$), $x = x_c$, and $x > x_c$ ($x = 3.5$). The high-density transition marking the onset of sublattice order is evident in each graph by an inflection that increases in intensity. At lower densities one can see an Ising-like inflection develop, giving for $x > x_c$ the typical van der Waals loops. Figure 14 shows p/kT for the same values of x used in Fig. 13 and one sees a kink in the curve at high densities (marking the sublattice transition) at all temperatures while at low densities and temperatures the typical Ising-like swallowtail behavior develops. One can see particularly in Fig. 14 for $x > x_c$ that there are two kinks in the p/kT versus y curve marking the gas-liquid and liquid-solid transitions. Figure 15 shows an enlargement of the upper

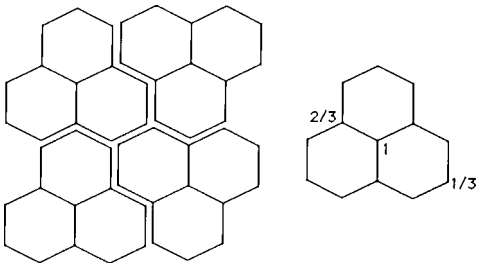


FIG. 12. The block of 13 lattice sites used for the generalized Bethe approximation on the honeycomb lattice. The set of four blocks indicates how the plane is covered with these blocks. The numbers on the single block indicate how much of each site belongs to the block.

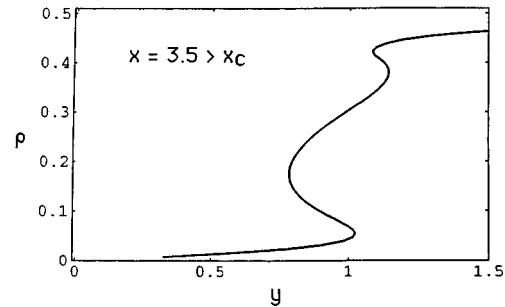
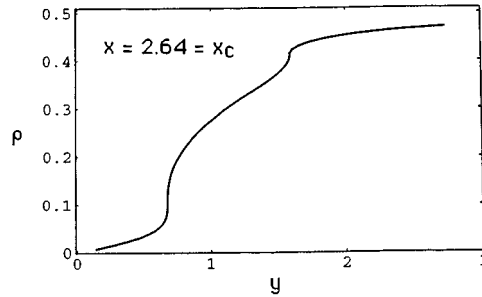
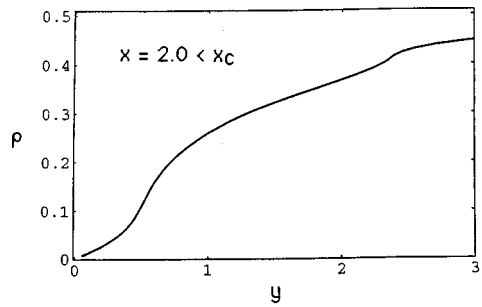


FIG. 13. The density as a function of activity (y) for the $\frac{9}{5}$ model in the Bethe approximation using the block of 13 lattice sites shown in Fig. 12. The critical value of x is $x_c = 2.64$ and shown are the isotherms for $x = 2.0 < x_c$, $x = x_c$, and $x = 3.5 > x_c$.

kink in the p/kT versus y curve of the $x > x_c$ case in Fig. 14 where one clearly sees that there is a curve crossing (though not quite as crisp as the swallowtail-like figure involved in the gas-liquid crossing) marking the switch from liquid to solid phases.

From the kinks in the p/kT versus y curve we can pick off the loci of the $y_\sigma(u)$ curves for the two phase transitions. These are shown in Fig. 16. The critical parameters are estimated to be $x_c = 2.64$ ($u_c = 0.379$), $y_c = 0.666$, and $\rho_c = 0.0959$. The triple point, where the two branches come together, is estimated to occur at $x_t = 4.17$ ($u_t = 0.24$) with $y_t = 0.986$ and $\rho_t = 0.312$. The labels a , b , and c in Fig. 16 refer to regions of the diagram that can be studied using different exact series, an approach which we will discuss in the next section. The critical point can be located quite accurately. One zooms in on the swallowtail crossing of the curves and the $\beta p(y)$ curves are fit to polynomials in the neighborhood of the crossing; the exact crossing point is then determined analytically as is the density (slope of each curve) on either side of the crossing point. The order parameter $R = \rho_H - \rho_L$ is used, plotting R^2 as a function of u (in the Bethe approximation the coexistence curve has the classical

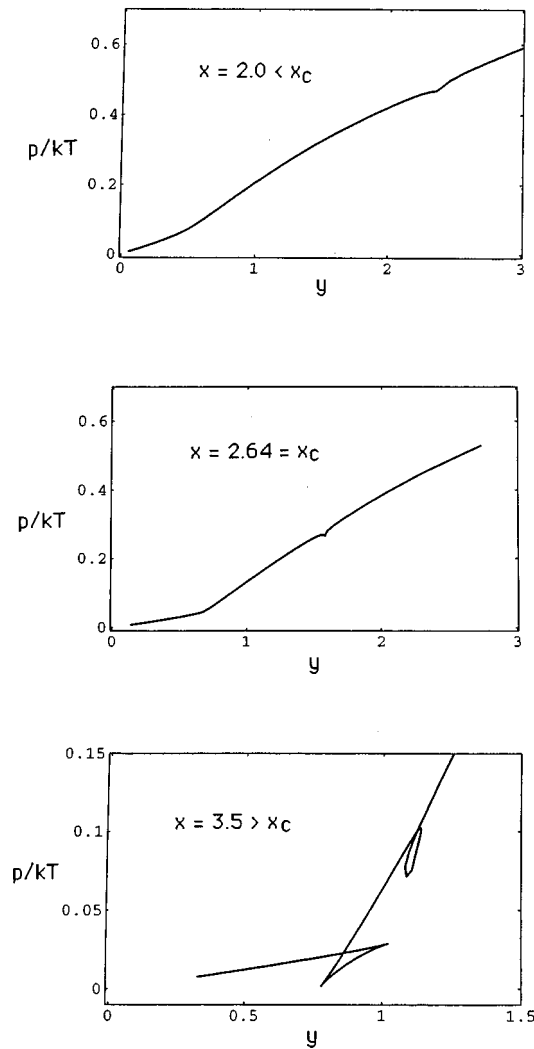


FIG. 14. The quantity p/kT as a function of activity (y) for the $\frac{9}{5}$ model in the Bethe approximation using the block of 13 lattice sites shown in Fig. 12. The curves represent the same values of x used in Fig. 13. For the case of $x=3.5 > x_c$ one clearly sees two first-order phase transitions, the gas-liquid transition at low density and the liquid-solid transition at high density.

exponent $\beta = \frac{1}{2}$ and so R^2 is linear in u . R^2 is then extrapolated linearly to zero, thus giving the critical value of u and also the critical density. We can treat the gas-solid transition in a similar manner, the main difference from it the gas-liquid transition being that a second-order transition persists to infinite temperature ($u=1$). The $\rho_\sigma(u)$ phase diagram so determined is shown in Fig. 17.

In the $\frac{9}{5}$ model the gas-liquid and liquid-solid transitions are distinct as seen in Fig. 13 and 14. It is of interest to see what happens when the 2 interaction of Fig. 6 is turned off (setting $\varepsilon_2=0$ or taking $v=1$). The behavior of the density and the pressure as a function of y when this is done is shown in Fig. 18 for the case of $x=2.5$. Now one sees that there is only one transition (gas-solid); this holds true at all temperatures. This then is the analog of the model on the square-planar lattice with nearest-neighbor exclusion and next-nearest-neighbor attraction of Fig. 3(b). The bonds in this case reinforce the triangular sublattice structure shown in Fig. 7 and there is no reason for a separate, more random,

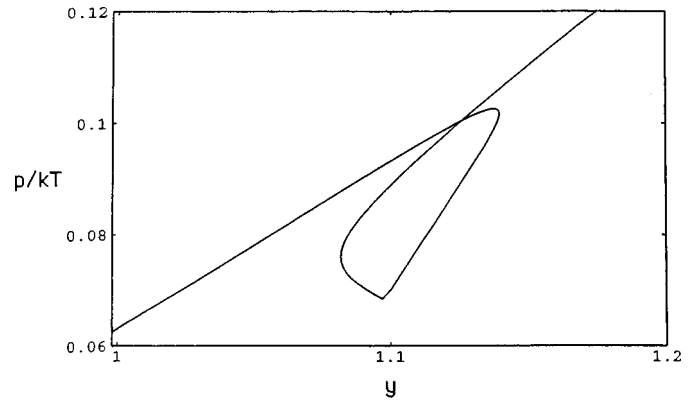


FIG. 15. An enlargement of the curve in Fig. 14 for $x=3.5$ showing the crossing of the liquid and solid p/kT curves as a function of y .

liquid phase to develop. The $y_\sigma(u)$ locus is shown in Fig. 19 for this system. Now one can clearly see that the transition changes from second order to first order at a tricritical point. Using the same numerical technique as described for the gas-liquid critical point in the $\frac{9}{5}$ model, we can accurately determine the density on each branch of the coexistence curve to give the $\rho_\sigma(u)$ phase-diagram and this is also shown in Fig. 19.

Having seen that the $\frac{9}{5}$ model on the honeycomb lattice shows gas/liquid/solid phase behavior, we want to see how much of this behavior we can substantiate using exact series. In the next section we review a simple method to obtain the series.

IV. ACTIVITY SERIES

In this section we review the method developed by Springgate and Poland [10] a number of years ago to obtain activity series for lattice models using transfer matrices. The basic idea is that one takes a strip of lattice of finite width as illustrated for the honeycomb lattice in Fig. 20(a). The fundamental quantity is then a finite vertical column of lattice sites as illustrated in Fig. 20(b). One uses periodic boundary

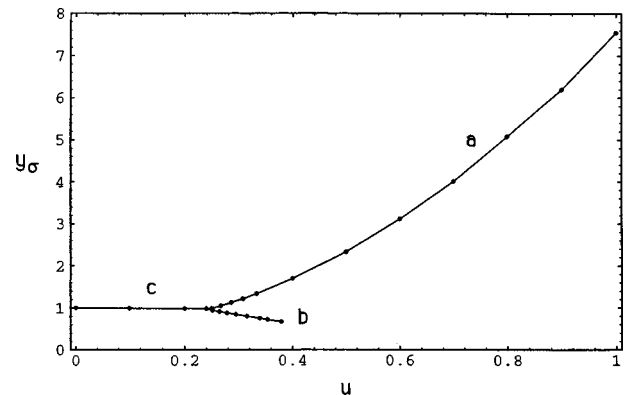


FIG. 16. The loci $y_\sigma(u)$ of the phase transition singularities in the activity as a function of the low-temperature parameter u ($=1/x$) for the $\frac{9}{5}$ model in the Bethe approximation. The loci are given by the curve crossing (p/kT versus y) as shown in Fig. 14. The letters a , b , and c label the branches of the function that can be determined by different series expansions.

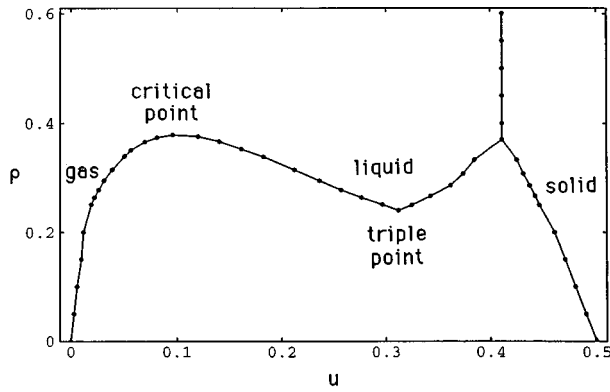


FIG. 17. The density-temperature phase diagram $\rho_\sigma(u)$, showing the loci of phase transition singularities for the $\frac{9}{5}$ model in the Bethe approximation. The values of the density are determined by the slopes of the crossing curves as shown in Fig. 14, evaluated at the crossing point.

conditions, indicated by the dashed lines in Fig. 20(a); one can imagine wrapping the strip into a cylinder. The cylinder can then be viewed as a set of consecutive rings of lattice sites. One then constructs a matrix \mathbf{W} that correlates all possible states (occupancy by particles) of one ring (the i th) with the states of the next ring (the $i+1$ st). For the case of eight sites in a ring as illustrated, all possible rings are shown in Fig. 20(c). Notice that the feature of nearest-neighbor exclusion has been used to reduce the number of possible rings. Also notice that one need use only one rotational position of each particle configuration, the matrix element representing

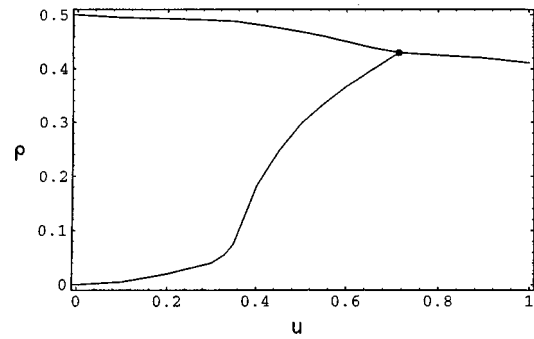
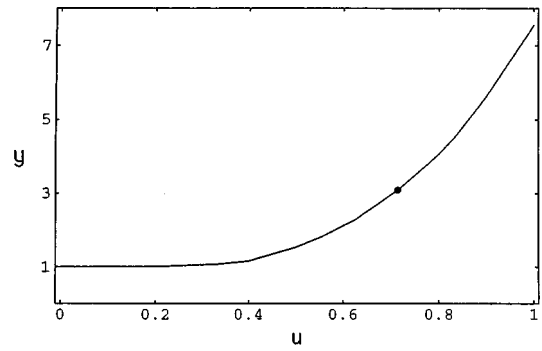


FIG. 19. The $y_\sigma(u)$ and $\rho_\sigma(u)$ phase diagrams for the case where $\nu=1$ in the Bethe approximation constructed using data similar to those shown in Fig. 18. At high temperatures there is a line of second-order transitions marking the onset of sublattice order. At a tricritical point (indicated in both graphs by a solid dot) the second-order transition becomes first order with a gas-solid coexistence curve.

one ring state followed by another including the contributions of all possible rotations; the use of symmetry reduced matrices was introduced by Runnels and Combs [11]. For the honeycomb lattice one sees that there is an alternating structure of the rings [see Fig. 20(b)] that also must be taken into account; because of this one can only use rings with an even number of sites.

The method then simply involves the multiplication of the matrices and extraction of the part of the grand partition function linear in the number of lattice sites (analog of the volume); this quantity is the coefficient b_n in the Mayer activity series for the pressure

$$\beta p = \sum_n b_n z^n. \quad (4.1)$$

For the case of nearest-neighbor interactions (attractive or repulsive) a finite ring with L sites will give the b_n exact for the doubly infinite planar lattice through $n=L-1$. The reason for this is that for L particles there can be a cyclic chain of interactions that go around the torus (due to the periodic boundary conditions) that is not present in the infinite system. Thus for the system with $L=8$ illustrated in Fig. 20 we obtain the first seven b_n exact for the particles with nearest-neighbor exclusion on the honeycomb lattice. The $\frac{9}{5}$ model illustrated in Fig. 5 has nearest-neighbor exclusion and next-nearest-neighbor attractions. For that model in order to get $m b$'s correct for the infinite lattice requires a ring with L

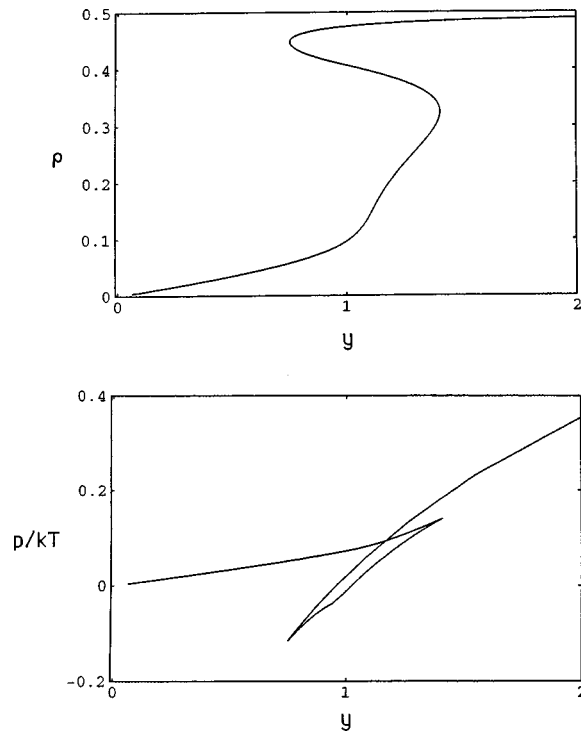


FIG. 18. The density and the pressure as a function of the fugacity for the model of Fig. 6 with $\nu=1$ ($\epsilon_2=0$) in the Bethe approximation. In this case there is only one curve crossing at any given temperature and a single gas-solid phase transition. The case shown is for $x=2.5$.

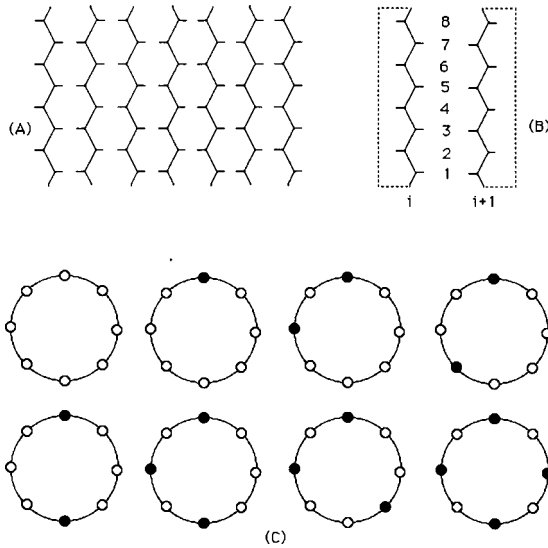


FIG. 20. Lattice configurations used to calculate exact series. (a) Illustration of a long row of vertical strips of lattice sites on the honeycomb lattice. (b) Nearest-neighbor vertical rows of lattice sites; the dashed lines indicate the periodic boundary conditions whereby the strip is wrapped into a torus. (c) The irreducible set of ring configurations (a ring circling the torus) required to construct the transfer matrix.

$=2(m+1)$ sites (for the same reasons just indicated for the case of nearest-neighbor interactions). Thus for the $L=8$ rings of Fig. 20 we will get only through $m=3$ of the b 's exact.

The matrix sizes (irreducible set of ring configurations) required for various L 's are $8 \times 8 (L=8)$, $26 \times 26 (L=12)$, $49 \times 49 (L=14)$, and $99 \times 99 (L=16)$. The largest matrix (for $L=16$) will give the b 's exact through $m=7$ for the $\frac{9}{5}$ model. This method also can give high-density series that represent perturbations about the perfect solid. In that case the series is in terms of the $1/z$, this quantity representing a hole in the perfect solid.

We now want to use activity series for the $\frac{9}{5}$ model to show that the features found in the Bethe approximation are also present in a more rigorous treatment of the model. We will focus on the $y_\sigma(u)$ phase diagram shown in Fig. 16. In that figure we have labeled various branches of the function by the letters a , b , and c . Each of these branches can be determined by a different type of series and we will treat these in turn.

A. a branch (high-density series)

The line of singularities indicated by a in Fig. 16 is most simply determined by using the high-density series. The high-density series has the form

$$\beta p_H = \frac{1}{2} \left[\ln(zx^3) + \sum_n b'_n(z')^n \right], \quad (4.2)$$

where

$$z' = \frac{1}{zx^6}. \quad (4.3)$$

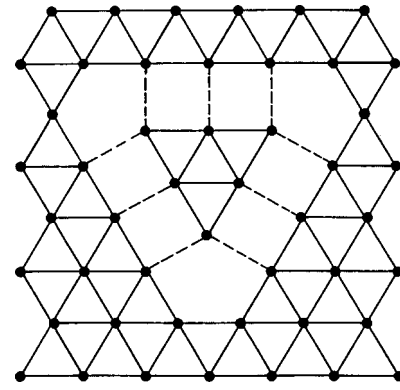


FIG. 21. The illustration of a perturbation in the perfect high-density solid caused by removing four particles and moving six particles onto the alternate sublattice. The dashed lines indicate v bonds.

The quantity z' represents an isolated hole introduced into the perfect solid. The z^{-1} term represents the removal of particle and the x^{-6} term represents the six bonds broken when a single particle is removed. Notice that z' is distinct from the definition of y in Eq. (1.11). The grand partition function for the perfect solid is written $\Xi = y^{M/2}$ [see Eq. (1.10)] since in the perfect solid every bond is shared by two particles (so we get x^3 instead of x^6).

The series for the general x - v model (not restricted to the $\frac{9}{5}$ model) through four terms is

$$\begin{aligned} b'_1 &= 1, & b'_2 &= (v/x)^3 - 3\frac{1}{2} + 3x, \\ b'_3 &= (v/x)^6 + 3(v/x)^4 - 12(v/x)^3 + 6(v^3/x^2) \\ &\quad + 3(v^2/x) + 19\frac{1}{3} - 30x + 9x^2 + 2x^3, \\ b'_4 &= (v/x)^9 + 9(v/x)^7 - 27\frac{1}{2}(v/x)^6 + 12(v/x)^5 \\ &\quad + 9(v^6/x^5) - 48(v/x)^4 + 9(v^5/x^4) + 130(v/x)^3 \\ &\quad + 15(v^4/x^3) - 3(v/x)^2 - 126(v^3/x^2) + 6(v^4/x^2) \\ &\quad - 42(v^2/x) + 30(v^3/x) - 129\frac{3}{4} + 3v + 18v^2 + 288x \\ &\quad + 9xv^2 - 178\frac{1}{2}x^2 + 5x^3 + 12x^4 + 3x^5. \end{aligned} \quad (4.4)$$

For the high-density series the relation between the ring size and the number of terms one gets exactly for the infinite lattice can be a little tricky since one is dealing not only with the range of bonds, as in the low-density case, but with the number of particles that can be rearranged when a given number of holes are introduced into the lattice. We take an empirical approach to this question, determining the series for $L=8, 12, 14$, and 16 and seeing how many terms are the same as L is increased. Comparing the results of $L=14$ and $L=16$ the first six of the high-density b 's are the same and we assume that for $L=16$ we are indeed getting seven exact b 's.

Notice that in the b 's given in Eq. (4.4) there are terms of the form $(v/x)^m$. The origin of these is illustrated in Fig. 21 where we illustrate the $(v/x)^9$ term in b'_4 . Four particles are removed from the perfect triangular structure and then six

additional particles are moved off of the dominant sublattice (breaking a net of nine x -type bonds) onto the other sublattice (forming a net of nine v -type bonds).

It is useful to change variables and convert Eq. (4.2) into a series in y and the appropriate low-temperature parameter. First we introduce the variable $y' = 1/y$, which, using Eqs. (1.11) and (4.3) can be written as follows:

$$y' = \frac{1}{zx^3} = (z')x^3. \quad (4.5)$$

For the $\frac{9}{5}$ model with $x = w^5$ and $v = w^9$ we have the low-temperature parameter

$$t = 1/w. \quad (4.6)$$

While we need to write the series in terms t , we will still refer to our previous low-temperature parameter u of Eq. (1.4), which is related to t by

$$u = 1/x = t^5. \quad (4.7)$$

With the variables y' and t defined above the series of Eq. (4.2) becomes

$$\beta p_h = \frac{1}{2} \left[\ln y' + \sum_n b'_n(t)(y')^n \right]. \quad (4.8)$$

The first seven $b'_n(t)$ are given in the Appendix.

In Sec. II we have already given the high-density activity series in the high-temperature limit of $x = v = 1$. The relation between the series for βp_H and the density (ρ) and modified compressibility (χ_H) are given in Eq. (2.2). The series for $\chi_H(z^{-1})$ and $\chi_H(\rho')$ are illustrated for the case of $x = v = 1$ in Eqs. (2.4) and (2.5). As an example of the behavior of the series at lower temperatures we have the following series for $D \ln \chi_H$ evaluated at $x = 3.8$ (this turns out to be the critical value of x for the $\frac{9}{5}$ model):

$$\begin{aligned} \frac{\partial \ln \chi_H}{\partial \ln y'} &= 1 + 2.371(y') + 2.323(y')^2 + 3.215(y')^3 \\ &+ 4.101(y')^4 + 5.193(y')^5 + 6.760(y')^6 + \dots \end{aligned} \quad (4.9)$$

The (3/3) Padé approximant gives $y'_\sigma = 0.788$ or $y_\sigma = 1.27$ (there is also a spurious root $1/y_\sigma = 0.365$ in the numerator and denominator that cancels).

Padé approximants to series such as illustrated in Eq. (4.9) have no trouble in picking up the singularities in y and ρ associated with the onset of sublattice order. The loci of these singularities as a function of x (or $u = 1/x$) are shown in Fig. 22. The points at the high-temperature limit ($u = 1$) have already been determined in Sec. II and are given in Eq. (2.7). The one thing that this analysis does not give is any indication of the nature of the phase transition changing from second order to first order. We assume that at the high-temperature limit the transition is second order and that the line of singularities associated with the freezing transitions remains second order at least for a range of values of x . The curve $y_\sigma(u)$ shown in Fig. 22 is then the a branch of the $\frac{9}{5}$

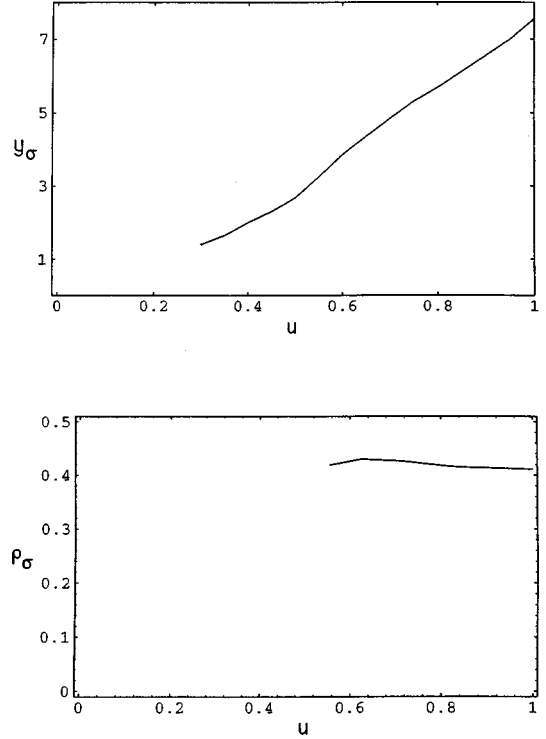


FIG. 22. The gas-solid part of the $y_\sigma(u)$ and $\rho_\sigma(u)$ phase diagrams for the $\frac{9}{5}$ models determined by $D \ln \chi_H$ using exact high-density series.

model shown in Fig. 16. We turn now to the b -branch associated with the gas-liquid critical point.

B. b branch (low-density series)

To determine the gas-liquid branch of the $y_\sigma(u)$ phase diagram we will utilize the low-density activity series. The first four b 's for general x and v are

$$\begin{aligned} b_1 &= 1, & b_2 &= -6\frac{1}{2} + 3x + 1\frac{1}{2}v, \\ b_3 &= 67\frac{1}{3} - 57x + 9x^2 + 2x^3 - 30v + 3v^2 + 12xv, \\ b_4 &= -850\frac{3}{4} + 1035x - 343\frac{1}{2}x^2 - 17x^3 + 12x^4 + 3x^5 \\ &+ 559\frac{1}{2}v - 113\frac{1}{4}v^2 + 7v^3 - 432xv^2 + 66x^2v \\ &+ 1\frac{1}{2}x^2v^2 + 9x^3v. \end{aligned} \quad (4.10)$$

Three more coefficients for the special case of the $\frac{9}{5}$ model are given in the Appendix [as $b_n(w)$].

The simplest way to see the development of a critical point is to follow the roots of the grand partition function in the complex- z (or $-y$) plane as the temperature is lowered from infinity. For all Ising models (single-site exclusion) at infinite temperature ($x = 1$) the grand partition function for a lattice of M sites is

$$\Xi = (1 + y)^M. \quad (4.11)$$

Setting $\Xi(y) = 0$ to obtain the roots of the grand partition function one has the result

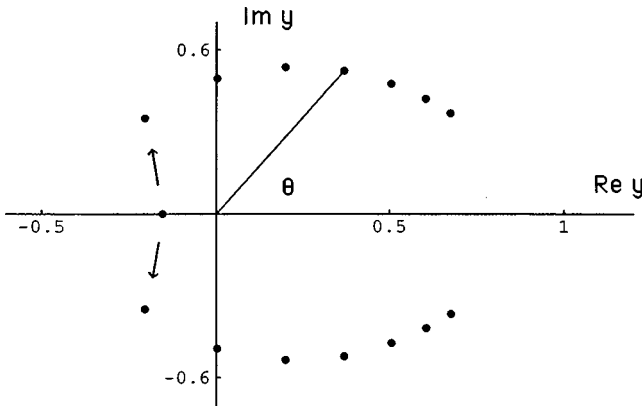


FIG. 23. The motion of the Lee-Yang roots of the grand partition function for the $\frac{9}{5}$ model as determined by $D \ln \chi_L$ using exact low-density series. At infinite temperature ($x=1$) the root closest to the origin is at $y_\sigma = -0.155$ and then, as the temperature is decreased, moves out into the complex- y plane. The points show increments of 0.2 in x for the range $x=1-2.4$. The angle θ is illustrated.

$$y_\sigma(x=1) = -1 \quad (M\text{-fold degenerate}). \quad (4.12)$$

As the temperature is lowered, y_σ moves from -1 out into the complex- y plane and finally, at the critical value of x touches onto the real positive y -axis at $y_\sigma = +1$.

All lattice gas models with nearest-neighbor exclusion exhibit a singularity on the negative activity axis close to the origin at high temperatures. The nature of the singularity at this point has been considered by Poland [12] and Lai and Fisher [13]. This means of course that at high temperatures activity series are not very well behaved since the radius of convergence is very small (in contrast, high temperature density series are well behaved).

For the $\frac{9}{5}$ model in the high-temperature limit Padé approximants of $D \ln \chi_L$ constructed from Eq. (2.10) give

$$y_\sigma = -0.155, \quad (4.13)$$

which is seen to be much closer to the origin than the result of Eq. (4.12) for Ising models. As the temperature is decreased one can follow this singularity out into the complex plane. To do this we use the Padé- $D \ln \chi_L$ method, using the seven $b_n(w)$ given in the Appendix plus three additional approximate terms. At lower temperatures the most important contribution to the b_n are from compact clusters (as illustrated by Fisher's cluster model [14] and a modification to include excluded volume effects [15]). The contribution of compact clusters will be correctly included in the approximate b_n we use (recall that it is linear clusters that stretch around the torus that are treated incorrectly). And in the high-temperature limit the approximate b_n are exact (the only interaction being nearest-neighbor exclusion). The motion of the roots in the complex- y plane is indicated in Fig. 23, where in the high-temperature limit one starts at y_σ given in Eq. (4.13) and, as the temperature is decreased, moves in the direction of the arrows around toward the real, positive y axis; points are shown for values of x starting at $x=1$ for the point of Eq. (4.13) and increasing in increments of 0.2 (the

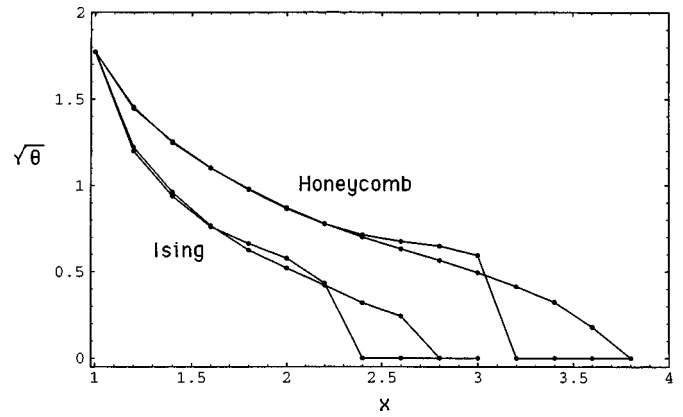


FIG. 24. The angle θ , as illustrated in Fig. 23, plotted as $\sqrt{\theta}$ versus x for the Ising model on the planar-triangular lattice (labeled as Ising) and for the $\frac{9}{5}$ model (labeled as Honeycomb) giving the results of $(\frac{4}{5})$ and $(\frac{5}{4})$ Padé approximants to $D \ln \chi_L$ using exact low-density series.

final value shown is for $x=2.4$). The angle θ that a point in the complex y plane makes with the real, positive y axis is also illustrated.

To compare the behavior of the $\frac{9}{5}$ model with that of the Ising model we have also used the 10 exact $b_n(x)$ that are known for the Ising model on the planar-triangular lattice [8]. For that case we determine the closest singularity to the real positive y axis using $D \ln \chi_L$. The value of the angle θ from the $(\frac{4}{5})$ and $(\frac{5}{4})$ approximants are then shown in Fig. 24 (plotting θ as a function of x). The known critical value of x for the Ising model on the triangular lattice is simply [16]

$$\text{(Ising model)} \quad x_c = 3. \quad (4.14)$$

One sees that one of the Padé approximants anticipates the locus on the real positive y axis, but that the other extrapolates smoothly to the known critical point. In Fig. 24 we also plot the same quantities for the $\frac{9}{5}$ model and one sees that one gets exactly analogous behavior simply shifted to lower temperatures. We estimate that the critical point occurs at

$$\left(\frac{9}{5} \text{ model}\right) \quad x_c = 3.8. \quad (4.15)$$

which represents a lower T_c than the value $x_c = 2.64$ found in the Bethe approximation (the Bethe approximation on the level of bonds gives $x_c = 4$ for the Ising critical point for the plane-square lattice while the exact value is $x_c = 5.828$).

The function $D \ln \chi_L$ is very well behaved at $x=x_c$ as shown below:

$$\begin{aligned} \frac{\partial \ln \chi_L}{\partial \ln y} &= 1 + 1.566y + 1.311y^2 + 1.531y^3 \\ &+ 1.378y^4 + 1.797y^5 + 1.570y^6 \\ &+ 1.854y^7 + 1.799y^8 + 2.074y^9 + \dots \end{aligned} \quad (4.16)$$

For $x > x_c$ ($T < T_c$) we can use the Padé- $D \ln \chi_L$ method to reliably give estimates of the gas-liquid $y_\sigma(u)$ locus (the b branch of Fig. 16). A few pairs (from $(\frac{4}{5})$ and $(\frac{5}{4})$ Padé approximants) are

$$x = 3.8 \quad y_\sigma = 0.951, 0.951,$$

$$\begin{aligned}
x=4.0 \quad y_\sigma &= 0.964, 0.966, \\
x=4.2 \quad y_\sigma &= 0.982, 0.987, \\
x=4.4 \quad y_\sigma &= 1.004, 1.011.
\end{aligned} \tag{4.17}$$

C. *c* branch (low- and high-density series)

The *c* branch of y_σ in Fig. 16 involves the phase transition separating gas and solid at very low temperatures. Recall that we picked a value of $\kappa < 2$ ($=9/5$) that guaranteed that the triangular-type solid of Fig. 7 would be the dominant phase at low temperatures. The condition for the equilibrium of gas and solid at low temperatures is that

$$\beta p_L(y_\sigma) = \beta p_H(y_\sigma). \tag{4.18}$$

We have already expressed βp_H as a function of $y' = 1/y$ and the low-temperature parameter $t = 1/w$ of Eq. (4.6). Likewise we can also express βp_L as a function of y and t so that both sides of Eq. (4.18) are written in terms of the same variables. Then we write $y_\sigma(t)$ as a series in powers of t ,

$$y_\sigma(t) = 1 + a_1 t + a_2 t^2 + \dots, \tag{4.19}$$

where the a 's are unknown coefficients. Using the known series [of Eqs. (4.1) and (4.8), both given in the Appendix], one inserts the form of Eq. (4.19) in both series (one is in powers of y the other in powers of $1/y$), and this then becomes a recursion relation for the a 's. This approach has been discussed in detail elsewhere [17–19]. Thus we can use the low and high-density activity series and determine the low-temperature expansion of the *c* branch of Fig. 16 explicitly through Eq. (4.19). One can also then use the form of Eq. (4.19) in the y series for the density on the low- and high-density sides to obtain the density along the low- and high-density sides of the phase diagram. We have the t series exact through the term in t^{35} as given below:

$$\begin{aligned}
y_\sigma &= 1 + t^{15} - t^{18} + 2t^{21} - t^{24} + 3t^{25} \\
&\quad + 5t^{27} - 6t^{28} - 3t^{29} - 5t^{30} + 15t^{31} \\
&\quad - 9t^{32} + 20t^{33} - 15t^{34} - 15t^{35} + \dots,
\end{aligned} \tag{4.20}$$

$$\begin{aligned}
\rho_L &= t^{15} + 3t^{21} + 6t^{25} + 9t^{27} - 6t^{30} \\
&\quad + 36t^{31} + 6t^{32} + 27t^{33} + 39t^{35} + \dots,
\end{aligned} \tag{4.21}$$

$$\begin{aligned}
\rho_H &= 1/2 - (1/2)t^{15} - t^{18} - 1(\frac{1}{2})t^{21} \\
&\quad - 2t^{24} - 3t^{25} - 2(\frac{1}{2})t^{27} - 9t^{28} \\
&\quad - 4(1/2)t^{29} - 2t^{30} - 18t^{31} - 22(\frac{1}{2})t^{32} \\
&\quad + 10t^{33} - 36t^{34} - 82(\frac{1}{2})t^{35} + \dots.
\end{aligned} \tag{4.22}$$

We emphasize that the above series are expansions along the low-temperature coexistence curve and not just low-temperature expansions of the fugacity and densities.

We have now determined the locus $y_\sigma(u)$ for each of the three branches of this function labeled in Fig. 16 and can now combine them to give the analogous figure, but this time constructed from the results of exact series rather than from

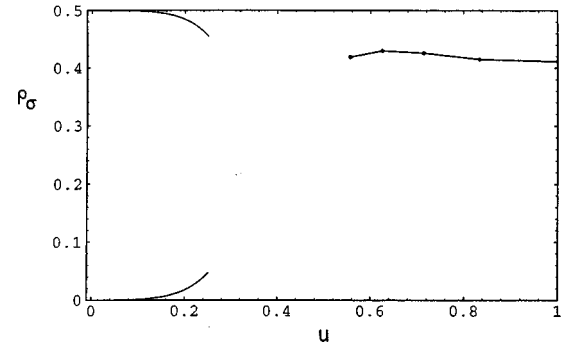
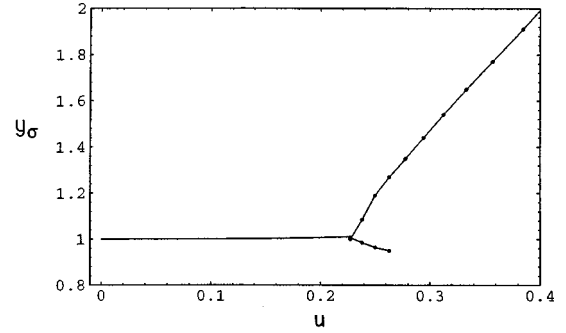


FIG. 25. The $y_\sigma(u)$ phase diagram and parts of the $\rho_\sigma(u)$ phase diagram for the $\frac{9}{5}$ model as determined by exact series. The behavior is qualitatively the same as shown in Fig. 16 for the Bethe approximation.

the Bethe approximation. The result is shown in Figure 25 where the *a*-branch comes from $D \ln \chi_H$ as illustrated in Fig. 22, the *b* branch comes from $D \ln \chi_L$, using the results shown in Eq. (4.17), and the *c* branch is a plot of Eq. (4.20). While the parameters for the critical point and the triple point are quantitatively different from those found in the Bethe approximation, the qualitative features of $y_\sigma(u)$ are the same. Our estimate of the critical-point and triple-point parameters are (showing those for the Bethe approximation for comparison) shown in Table I.

The qualitative agreement between the $y_\sigma(u)$ phase diagrams gives us some confidence that the generalized Bethe approximation is a useful tool to describe the pattern of singularities represented by $y_\sigma(u)$ in systems with multiple phases and phase transitions.

The $\rho_\sigma(u)$ phase-diagram is also shown in Fig. 25 (the analog of Fig. 17). In this case series expansions cannot give the full picture simply because we have no series representing the liquid phase (and hence the center of the figure is blank). We can follow the locus of the second-order gas-

TABLE I. Critical point and triple-point parameters.

| | Critical point | Triple point |
|--------|---|---|
| Series | $x_c = 3.80$ ($u_c = 0.263$) $y_c = 0.950$ | $x_t = 4.40$ ($u_t = 0.227$) $y_t = 1.008$ |
| Bethe | $x_c = 2.64$ ($u_c = 0.379$) $y_c = 0.666$ | $x_t = 4.17$ ($u_t = 0.240$) $y_t = 0.986$ |

solid transition from high temperatures downward as shown in Fig. 22 and we have the high- and low-density branches of the gas-solid coexistence curve at low temperatures, as given by Eqs. (4.21) and (4.22). In particular, we have no estimate of the location of the tricritical point where the gas-solid transition switches from second order to first order (if indeed it does) and we have no estimate of the triple-point density.

One of the main features of the present model is the inclusion of two types of bonding that lead to very different geometries for clusters as illustrated in Fig. 8. In particular, the presence of a liquid phase can be attributed to the occurrence of random combinations of the two types of bonding as illustrated in Fig. 8(b). It is of interest therefore to quantitatively determine the extent of each type of bonding. We can do this readily for an infinitely long torus of lattice sites with a finite circumference, as illustrated in Fig. 20. For this case the grand partition function is given in terms of the transfer matrix \mathbf{W} that correlates the possible states of nearest-neighbor rings on the torus,

$$\Xi = \text{Tr } \mathbf{W}^L \quad (4.23)$$

where L is the length of the torus. The density is then given by

$$\left(\lim_{L \rightarrow \infty} \right) \rho = \frac{\text{Tr } \mathbf{W}' \mathbf{W}^{L-1}}{\text{Tr } \mathbf{W}^L} \quad (4.24)$$

where

$$\mathbf{W}' = \frac{\partial \mathbf{W}}{\partial \ln z}. \quad (4.25)$$

The limit $L \rightarrow \infty$ is achieved by increasing L until the result is independent of L . One can also calculate the density of bonds by replacing the variable z in Eq. (4.27) with either x or v to give the density of the two types of bonds. We define the bond density as the density of a particular type of bond per particle,

$$R_x = \rho_x / \rho \quad \text{and} \quad R_v = (9/5) \rho_v / \rho. \quad (4.26)$$

Note that for comparison we multiply ρ_v by $\frac{9}{5}$ since the v bonds represent an energy that is $\frac{9}{5}$ that of the x bonds.

The quantities R_x and R_v are plotted as a function of ρ at the critical value of x ($x_c = 3.8$) in Fig. 26. One sees that at low density most of the bonding is of the v type, but as the density of particles increases the x type of bonding starts to predominate and as one approaches the limit of close packing all of the bonding is of the x type. So clearly both types of bonding play an important role with a shift from one type to the other as the density increases.

Finally we want to show that the gas/liquid/solid phase diagram collapses to a gas/solid phase diagram if one turns off the v type bonds (setting $\varepsilon_2 = 0$ or $v = 1$). We have already shown this in the Bethe approximation, as illustrated in Fig. 19. We determine $y_\sigma(u)$ in this case by using the Padé- $D \ln \chi$ method using high- and low-density series, as before. The points that we obtain reliably in this case are shown in Fig. 27. The almost straight line at low u is the low-temperature locus of $y_\sigma(u)$ obtained as in Eq. (4.19). We have this series exactly through u^{10} as given below:

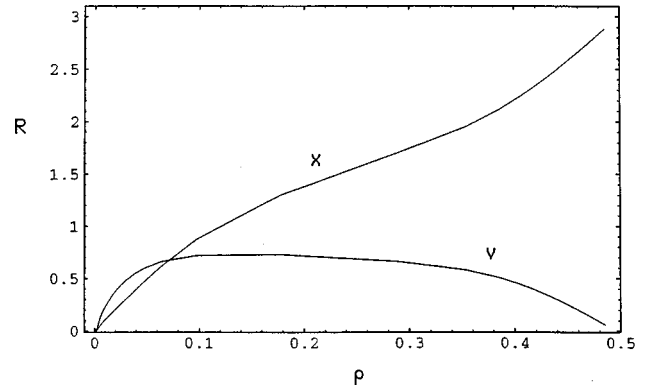


FIG. 26. The bond density as defined in Eq. (4.28) for x and v bonds at the critical isotherm, $x_c = 3.8$, as a function of density for an infinite torus with a circumference of 12 lattice sites (as illustrated in Fig. 20).

$$y_\sigma = 1 + u^3 + 3u^5 - u^6 + 12u^7 - 12u^8 + 61u^9 - 105u^{10} + \dots, \quad (4.27)$$

$$\rho_L = u^3 + 6u^5 - 3u^6 + 39u^7 - 42u^8 + 282u^9 - 447u^{10} + \dots, \quad (4.28)$$

$$\rho_H = \frac{1}{2} - \left(\frac{1}{2}\right)u^3 - 3u^5 + u^6 - 19\left(\frac{1}{2}\right)u^7 + 13\left(\frac{1}{2}\right)u^8 - 137u^9 + 141u^{10} + \dots. \quad (4.29)$$

Presumably we could link the separate regions shown in Fig. 27 into a continuous curve if we had longer exact series.

V. DISCUSSION

In this paper we have treated the model illustrated in Fig. 5 and 6, with parameters given in Eqs. (1.15) and (1.16), the $\frac{9}{5}$ model. The essential feature of the model is that at high density and low temperature the triangular-type solid shown in Fig. 7 will be the stable phase [the choice of parameters in Eqs. (1.15) and (1.16) guarantees this]. Since there is nearest-neighbor exclusion in the model there will be a fluid-solid transition of some type at all temperatures marking the onset of sublattice order (in a second-order transition) or

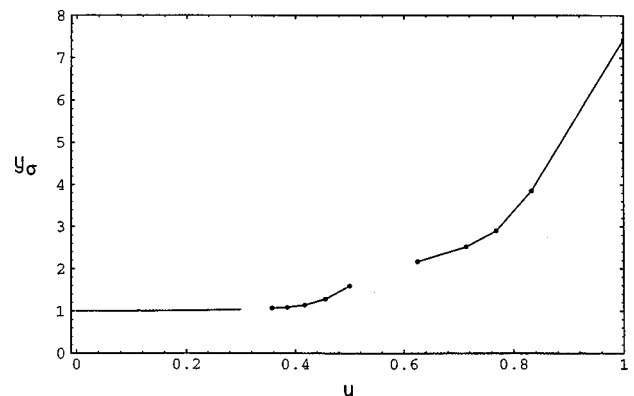


FIG. 27. The $y_\sigma(u)$ and $\rho_\sigma(u)$ phase diagrams for the case when $v = 1$ as determined by exact series. As with the Bethe approximation of Fig. 19, there is a single gas-solid transition at all temperatures.

marking a discontinuous jump in sublattice order (in a first-order phase transition). The presence of a liquid phase is made likely by the inclusion of two different modes of bonding (x -type and v -type bonds) that, at intermediate values of density and temperature, lead to mixed types of clusters as illustrated in Fig. 8(b); the presence of both types of bonding is documented in Fig. 26.

In the generalized Bethe approximation this model does indeed show gas, liquid, and solid phases with a standard gas-liquid critical point (as illustrated in Figs. 16 and 17). In their famous paper on phase transitions, Lee and Yang [4] give a figure (Fig. 2 in their Ref. [1]) showing pressure as a function of activity, the curve having two kinks in it that represent the location of the two singular points (where the density is discontinuous) representing the gas-liquid and liquid-solid phase transitions. Our Fig. 14 (for $x=3.5$) is a realization of the schematic figure of Lee and Yang for a specific model (the $\frac{9}{5}$ model); of course one must imagine removing the swallowtail cusps from our Fig. 14 (the equivalent of using Maxwell's construction for the van der Waals loops).

We have already reviewed the evidence obtained from exact series expansions that shows that the presence of gas, liquid, and solid phases in the model is not just an artifact of the Bethe approximation. The key point in the evidence that the $\frac{9}{5}$ model does have a standard liquid phase is that at x_c

$=3.8$ the functions $\chi_L(y)$ and $\chi_H(y^{-1})$ give distinctly different values of y_σ . The series for $D \ln \chi_H(y^{-1})$ is given in Eq. (4.9) while the series for $D \ln \chi_L(y)$ is given in Eq. (4.16), both for $x_c=3.8$. Both of these series are very well behaved and so the y_σ values obtained from them are very reliable. But it is not just a single pair of values of y_σ that convinces, but the trends of the numbers as a function of temperature. And it is clear in Fig. 25 that there are distinct branches to the $y_\sigma(u)$ function.

Thus this model supports the use of the generalized Bethe approximation to give qualitatively correct phase diagrams for complex systems. One advantage of the Bethe approximation is that the entire range of density and temperature can be treated using a single, very simple formalism. Another is that a first-order phase transition shows up clearly as a swallowtail cusp in $\beta p(y)$ (first-order phase transitions are difficult to describe using series).

Finally we note that in our model the gas-solid transition is second order at high temperatures. There is evidence in the literature [20] that if the extent of the repulsive core in lattice gases is made greater (or, equivalently, if the lattice grid is made finer) the sublattice-order transition is first order at high temperature. Thus there is the possibility that a model only somewhat more complex than the present one can be constructed that shows a gas-liquid critical point and a first-order fluid-solid transition for all temperatures.

APPENDIX

Low- and high-density activity series for the $\frac{9}{5}$ model; $x=w^5$ and $v=w^9$.

1. Low-density series

$$b_1 = 1,$$

$$b_2 = -6\left(\frac{1}{2}\right) + 3w^5 + 1\left(\frac{1}{2}\right)w^9,$$

$$b_3 = 67\left(\frac{1}{3}\right) - 57w^5 - 30w^9 + 9w^{10} + 12w^{14} + 2w^{15} + 3w^{18},$$

$$b_4 = -850\left(\frac{3}{4}\right) + 1035w^5 + 559\left(\frac{1}{2}\right)w^9 - 343\left(\frac{1}{2}\right)w^{10} - 432w^{14} - 17w^{15} - 113\left(\frac{1}{4}\right)w^{18} + 66w^{19} \\ + 12w^{20} + 39w^{23} + 9w^{24} + 3w^{25} + 7w^{27} + 1\left(\frac{1}{2}\right)w^{28},$$

$$b_5 = 12\,009\left(\frac{1}{5}\right) - 18\,987w^5 - 10\,434w^9 + 9\,666w^{10} + 11\,859w^{14} - 886w^{15} + 3\,192w^{18} \\ - 3\,780w^{19} - 435w^{20} - 2\,235w^{23} - 48w^{24} - 21w^{25} - 406w^{27} + 273w^{28} + 96w^{29} + 21w^{30} \\ + 126w^{32} + 48w^{33} + 15w^{34} + 6w^{35} + 18w^{36} + 6w^{37} + 3w^{38},$$

$$b_6 = -181\,974\left(\frac{1}{6}\right) + 353\,541w^5 + 196\,450\left(\frac{1}{2}\right)w^9 - 242\,956\left(\frac{1}{2}\right)w^{10} - 294\,267w^{14} \\ + 54\,120w^{15} - 80\,527\left(\frac{1}{2}\right)w^{18} + 144\,190\left(\frac{1}{2}\right)w^{19} + 7525\left(\frac{1}{2}\right)w^{20} + 85\,170w^{23} \\ - 15\,681w^{24} - 2058w^{25} + 15\,625\left(\frac{1}{2}\right)w^{27} - 24\,610\left(\frac{1}{2}\right)w^{28} - 4680w^{29} - 805w^{30} \\ - 10\,101w^{32} - 609w^{33} + 24w^{34} - 57w^{35} - 1425w^{36} + 1029w^{37} + 501w^{38} + 184\left(\frac{1}{2}\right)w^{39} \\ + 42w^{40} + 408w^{41} + 207w^{42} + 93w^{43} + 33w^{44} + 60\left(\frac{1}{2}\right)w^{45} + 24w^{46} + 19\left(\frac{1}{2}\right)w^{47} \\ + 7\left(\frac{1}{2}\right)w^{48} + \left(\frac{1}{2}\right)w^{54},$$

$$\begin{aligned}
b_7 = & 2\,896\,711\left(\frac{1}{7}\right) - 6\,671\,337w^5 - 3\,736\,740w^9 + 5\,774\,967w^{10} + 6\,941\,790w^{14} \\
& - 2\,017\,733w^{15} + 1\,921\,239w^{18} - 4\,607\,991w^{19} + 34\,326w^{20} - 2\,719\,155w^{23} \\
& + 1\,055\,844w^{24} + 100\,803w^{25} - 502\,847w^{27} + 1\,249\,137w^{28} + 86\,922w^{29} \\
& + 10\,352w^{30} + 499\,149w^{32} - 123\,591w^{33} - 35\,724w^{34} - 4305w^{35} + 70\,257w^{36} \\
& - 131\,517w^{37} - 35\,445w^{38} - 8742w^{39} - 1749w^{40} - 42\,531w^{41} - 4956w^{42} - 255w^{43} \\
& - 48w^{44} - 5062w^{45} + 3624w^{46} + 2151w^{47} + 1023w^{48} + 408w^{49} + 1407w^{50} \\
& + 858w^{51} + 525w^{52} + 234w^{53} + 185w^{54} + 117w^{55} + 90w^{56} + 48w^{57} + 21w^{58} \\
& + 6w^{59} + w^{60} + 3w^{61} + 3w^{63}.
\end{aligned}$$

2. High-density series ($t = 1/w$)

$$b'_1 = t^{15},$$

$$b'_2 = t^{18} + 3t^{25} - 3\left(\frac{1}{2}\right)t^{30},$$

$$b'_3 = t^{21} + 6t^{28} + 3t^{29} + 2t^{30} + 3t^{32} - 12t^{33} + 9t^{35} - 30t^{40} + 19\left(\frac{1}{3}\right)t^{45},$$

$$\begin{aligned}
b'_4 = & t^{24} + 9t^{31} + 9t^{32} + 3t^{33} + 3t^{34} + 12t^{35} - 27\left(\frac{1}{2}\right)t^{36} + 6t^{37} + 30t^{38} + 18t^{39} + 24t^{40} + 18t^{42} \\
& - 126t^{43} - 48t^{44} + 5t^{45} + 3t^{46} - 42t^{47} + 127t^{48} - 178\left(\frac{1}{2}\right)t^{50} + 288t^{55} - 259\left(\frac{1}{2}\right)t^{60},
\end{aligned}$$

$$\begin{aligned}
b'_5 = & t^{27} + 12t^{34} + 18t^{35} + 6t^{36} + 3t^{37} + 24t^{38} - 46t^{39} + 12t^{40} + 75t^{41} + 93t^{42} + 102t^{43} + 36t^{44} \\
& + 123t^{45} - 315t^{46} - 231t^{47} + 82t^{48} + 66t^{49} - 144t^{50} + 555t^{51} - 993t^{53} - 474t^{54} - 420t^{55} \\
& + 18t^{56} - 456t^{57} + 2007t^{58} + 603t^{59} - 679t^{60} - 48t^{61} + 483t^{62} - 1309t^{63} + 2637t^{65} \\
& - 2796t^{70} + 971\left(\frac{1}{5}\right)t^{75},
\end{aligned}$$

$$\begin{aligned}
b'_6 = & t^{30} + 15t^{37} + 30t^{38} + 11t^{39} + 3t^{40} + 39t^{41} - 74\left(\frac{1}{2}\right)t^{42} + 15t^{43} + 138t^{44} + 251t^{45} + 324t^{46} \\
& + 135t^{47} + 363t^{48} - 480t^{49} - 726t^{50} + 306t^{51} + 726t^{52} - 57t^{53} + 2082\left(\frac{1}{3}\right)t^{54} + 627t^{55} \\
& - 3105t^{56} - 3129t^{57} - 2815\left(\frac{1}{2}\right)t^{58} - 234t^{59} - 3443t^{60} + 7842t^{61} + 4800t^{62} - 5509t^{63} \\
& - 3662\left(\frac{1}{2}\right)t^{64} + 495t^{65} - 8752t^{66} - 2412t^{67} + 21\,561t^{68} + 8730t^{69} + 3436\left(\frac{1}{2}\right)t^{70} \\
& - 522t^{71} + 7902t^{72} - 28\,275t^{73} - 6972t^{74} + 16\,789t^{75} + 597t^{76} - 5247t^{77} + 13\,430t^{78} \\
& - 34\,920t^{80} + 27\,555t^{85} - 7796\left(\frac{2}{3}\right)t^{90},
\end{aligned}$$

$$\begin{aligned}
b'_7 = & t^{33} + 18t^{40} + 45t^{41} + 15t^{42} + 6t^{43} + 60t^{44} - 114t^{45} + 30t^{46} + 213t^{47} + 489t^{48} + 780t^{49} \\
& + 318t^{50} + 811t^{51} - 486t^{52} - 1782t^{53} + 867t^{54} + 2808t^{55} + 1263t^{56} + 6971t^{57} \\
& + 3372t^{58} - 5703t^{59} - 10\,638t^{60} - 12\,315t^{61} + 1383t^{62} - 10\,769t^{63} + 22\,035t^{64} + 27\,783t^{65} \\
& - 21\,667t^{66} - 33\,957t^{67} - 13\,743t^{68} - 53\,594t^{69} - 32\,832t^{70} + 91\,272t^{71} + 76\,203t^{72} \\
& + 37\,572t^{73} - 16\,686t^{74} + 61\,001t^{75} - 158\,604t^{76} - 93\,273t^{77} + 168\,493t^{78} + 94\,290t^{79} \\
& + 8049t^{80} + 120\,881t^{81} + 70\,827t^{82} - 387\,363t^{83} - 136\,644t^{84} + 17\,532t^{85} + 9759t^{86} \\
& - 116\,892t^{87} + 372\,342t^{88} + 77\,679t^{89} - 307\,235t^{90} - 6831t^{91} + 55\,824t^{92} - 138\,040t^{93} \\
& + 437\,997t^{95} - 275\,184t^{100} + 65\,718\left(\frac{1}{7}\right)t^{105}.
\end{aligned}$$

- [1] D. Poland, Phys. Rev. E **59**, 1512 (1999).
- [2] L. Onsager, Phys. Rev. **65**, 117 (1944).
- [3] J. Orban, J. Van Crean, and A. Bellemans, J. Chem. Phys. **49**, 1778 (1968).
- [4] T. D. Lee and C. N. Yang, Phys. Rev. **87**, 404 (1952); **87**, 410 (1952).
- [5] D. S. Gaunt and M. E. Fisher, J. Chem. Phys. **43**, 2840 (1965).
- [6] A. Bellemans and R. K. Nigam, J. Chem. Phys. **46**, 3237 (1967).
- [7] M. W. Springgate and D. Poland, Phys. Rev. A **20**, 1267 (1979).
- [8] M. F. Sykes, J. W. Essam, and D. S. Gaunt, J. Math. Phys. **6**, 283 (1965).
- [9] M. F. Sykes, D. S. Gaunt, S. R. Mattingly, J. W. Essam, and C. J. Elliott, J. Math. Phys. **14**, 1066 (1973).
- [10] M. W. Springgate and D. Poland, J. Chem. Phys. **62**, 680 (1975).
- [11] L. K. Runnels and L. L. Combs, J. Chem. Phys. **45**, 2482 (1966).
- [12] D. Poland, J. Stat. Phys. **35**, 341 (1984).
- [13] S-N. Lai and M. E. Fisher, J. Chem. Phys. **103**, 8144 (1995).
- [14] M. E. Fisher, Physics (Long Island City, N.Y.) **3**, 255 (1967).
- [15] P. K. Swaminathan and D. Poland, J. Chem. Phys. **69**, 3660 (1978).
- [16] See: H. S. Green and C. A. Hurst, *Order-Disorder Phenomena* (Interscience, 1964); Chapter 5. Using magnetic language, the critical value of $K (= \beta J)$ for isotropic interactions is given by the condition that $3(\sinh 2K)^2 = 1$ for the triangular lattice, $\sinh(2K) = 1$ for the square planar lattice and $3(\tanh K)^2 = 1$ for the honeycomb lattice (called the hexagonal lattice by Green and Hurst). In all cases the conversion to lattice gas language is given by $x_c = \exp(4K_c)$ where $x = \exp(-\varepsilon/kT)$ where ε is the nearest-neighbor interaction energy.
- [17] D. Poland, Phys. Rev. B **28**, 5285 (1983).
- [18] D. Poland, Phys. Rev. B **29**, 4130 (1984).
- [19] D. Poland, J. Chem. Phys. **80**, 2767 (1984).
- [20] J. Orban and A. Bellemans, J. Chem. Phys. **49**, 363 (1968).